Designing the observation sliding mode combined with the PID controller to estimate the speed of the IM optimized by PSO algorithm

Thinh Cong Tran[1,*], *Hau Huu Vo*[2], *Pavel Brandstetter*[3]

[1]Modeling Evolutionary Algorithms Simulation and Artificial Intelligence, Faculty of Electrical and Electronics Engineering, Ton Duc Thang University, Ho Chi Minh City, Vietnam.
[2]Faculty of Electrical and Electronics Engineering, Ton Duc Thang University, Ho Chi Minh City, Vietnam.
[3]Faculty of Electrical Engineering and Computer Science, VSB–Technical University of Ostrava, Czech Republic.

*Corresponding Author: Thinh Cong Tran (email:trancongthinh@tdtu.edu.vn)
(Received: 28-October-2024; accepted: 06-March-2024; published: 31-March-2025)
http://dx.doi.org/10.55579/jaec.202591.474

Abstract. *The paper presents a solution combining the sliding mode observer (SMO) with the PID controller to improve the accuracy of speedy estimation of the induction motor (IM) compared to the original sliding mode observer. The SMO's advantages include stability and sustainability, even in noisy environments or when system parameters change over time. In addition, the paper also proposes a new solution to optimize the SMO-PID controller using the particle swarm optimization (PSO) algorithm to increase the accuracy of speedy estimation compared to the traditional method. The paper covers the SMO algorithm, the SMO speed estimation model for IM motor controlled by the FOC method, the method of combining SMO with traditional PID controller, the SMO-PID controller with optimized parameters by applying PSO algorithm and comparing the results achieved by the two mentioned methods. Simulation results prove that the SMO-PID method using the PSO algorithm has superior advantages over the traditional SMO-PID method.*

Keywords: *Sliding mode observer, PID, PSO, Estimation, Induction motor, FOC.*

1. Introduction

Induction motors play an important role in the country's industry, so many studies exist on this motor. In the speedy estimation field of induction motors, there are many studies on the MRAS, Kalman, and sliding mode observer (SMO), soft computing methods that are fuzzy networks, artificial neural networks, etc. which are very complex to apply in the real world.

In MRAS, state variables from a reference model are compared to the estimated state variables from an adaptive model. An adaptation tool uses the difference between these state variables, and the output adjusts the adaptive model until it is implemented well [1–6]. The noise and parameter variations are sensitive to the drawbacks of MRAS.

For linear system models with additive independent white noise in both the transition and measurement systems, the Kalman filter is the best estimation method. Sadly, the majority of systems in use are nonlinear. The extended version of the Kalman filter (EKF) known as the EKF is used for systems that are not well-known, or whose models are not accurate [7–9]. However, the filter may quickly diverge if the process is modeled incorrectly or the initial estimation of the state is incorrect.

The outstanding advantage of the sliding mode observer (SMO) is its stability and sustainability even when the system has noise or when the parameters of the system change over time [10–13], [14] and [15]. However, if the amplitude of the control law changes too much, it can cause the system to oscillate (chattering) and become unstable. This article proposes a sliding mode observer for induction motors that integrates components of a PID controller to enhance accuracy and stability. Traditionally, determining the parameters Kp, Ki, and Kd of the PID controller is time-consuming and often yields limited accuracy. To address this issue, the paper introduces a soft computing algorithm to identify optimal parameters for the PID controller. While some algorithms, such as the genetic algorithm (GA), may not produce satisfactory solutions [7], and the Comprehensive Search Algorithm (CSA) can be complex with long convergence times [16], this paper opts for the Particle Swarm Optimization (PSO) algorithm. The solutions generated by the PSO algorithm, which were simulated using MATLAB Simulink, demonstrate a significant improvement in speed response compared to traditional PID-SMO speed estimation methods.

The paper's solution is implemented on an induction motor with the selected vector control method. Vector control (Field Oriented Control-FOC) is a modern control method widely used in electric drive systems, especially for induction motors. This method allows precise and efficient control of the motor's torque and speed, which is superior to traditional control methods. The model is implemented in the rotation coordinate system. The torque and the rotor flux are considered two independent vectors. This allows us to control both components independently, achieving high speed and torque control accuracy , [16–18]. The advantages of this method are high efficiency, precise control, good stability, and fast response.

The article includes an introduction to the mathematical model of observing the speed of an induction motor using a sliding model combined with a PID controller, an observation model applied to an induction motor using the FOC method, the particle swarm optimization (PSO) algorithm, its application to the model to find the optimal parameters for the PID controller, and finally the simulation results on an induction motor with many different speed levels in the cases of the load and no load.

2. Mathematical model, control structure, and algorithm

2.1. The mathematical model of the SMO speed observer with the IM according to the FOC method

Equations are used to rewrite the mathematical description of an induction motor using a state space.

$$\begin{aligned} \dot{x} &= A.x + B.u \\ y &= C.x \end{aligned} \tag{1}$$

where $x = [i_{S\alpha}\ i_{S\beta}\ \psi_{R\alpha}\ \psi_{R\beta}]^T$ is a state vector, $u = \begin{bmatrix} u_{S\alpha} & u_{S\beta} \end{bmatrix}^T$ is control vector, the output vector is y , and $\mathbf{A}$, $\mathbf{B}$, and $\mathbf{C}$ are the state matrix. Eqs 2 and 3 provide definitions of the matrix $\mathbf{A}$, $\mathbf{B}$, and $\mathbf{C}$.

$$A = \begin{bmatrix} a_{11} & a_{12} & a_{13} & a_{14} \\ a_{21} & a_{22} & a_{23} & a_{24} \\ a_{31} & a_{32} & a_{33} & a_{34} \\ a_{41} & a_{42} & a_{43} & a_{44} \end{bmatrix} \tag{2}$$

$$\mathbf{B} = \frac{1}{\sigma \cdot L_S} \cdot \begin{bmatrix} 1 & 0 & 0 & 0 \\ 0 & 1 & 0 & 0 \end{bmatrix}^T ; \mathbf{C} = \begin{bmatrix} 1 & 0 & 0 & 0 \\ 0 & 1 & 0 & 0 \end{bmatrix} \tag{3}$$

The values of the elements in the A is

$$\begin{aligned} a_{11} = a_{22} &= -\frac{(L_m^2 \cdot R_R + L_R^2 \cdot R_S)}{\sigma \cdot L_S \cdot L_R^2}; a_{12} = a_{21} = 0 \\ a_{13} = a_{24} &= \frac{L_m \cdot R_R}{\sigma \cdot L_S \cdot L_R^2}; a_{14} = -a_{23} = \frac{L_m \cdot \omega_R}{\sigma \cdot L_S \cdot L_R} \\ a_{31} = a_{42} &= \frac{L_m \cdot R_R}{L_R}; a_{32} = a_{41} = 0; \\ a_{33} = a_{44} &= -\frac{R_R}{L_R}; a_{34} = -a_{43} = -\omega_R \end{aligned} \tag{4}$$

Eq.4 [14] provides the sliding mode observer.

$$\begin{aligned} \dot{\hat{x}} &= \hat{\mathrm{A}}.\hat{x} + \mathrm{B}.u + G.\mathrm{sign}(S) \\ \hat{y} &= C.\hat{x} \end{aligned} \tag{5}$$

Where the expected state vector is $\hat{x}$, the output vector is $\hat{y}$, the output matrix is $\hat{\mathrm{A}}$, the coefficients matrixes are B, C and the gain matrix of the SMO, Eq.6 is G. In Eq.5, $\hat{\mathrm{A}}$is the probable parameters and A in Eq.1 is the real parameters.

$$G = \begin{bmatrix} g_{11} & g_{21} & g_{31} & g_{41} \\ g_{12} & g_{22} & g_{32} & g_{42} \end{bmatrix}^T \tag{6}$$

The equation representing the sliding surface is as follows:

$$S = y - \hat{y} = \begin{bmatrix} i_{S\alpha} - \hat{i}_{S\alpha} \\ i_{S\beta} - \hat{i}_{S\beta} \end{bmatrix} \tag{7}$$

From Eq.7, we have its derivative as Eq.8 and Eq.9.

$$\dot{S} = y - \dot{\hat{y}} = C.\dot{x} - C.\dot{\hat{x}} \tag{8}$$

$$\dot{S} = C.(A.\tilde{x} + (A - \hat{A})\hat{x} - G.sign(y - \hat{y})) \tag{9}$$

With $\tilde{\mathbf{X}} = \mathbf{X} - \widehat{\mathbf{X}}$ and $\mathbf{A} - \hat{\mathbf{A}}$ that is calculated as the expression Eq.10

$$\mathbf{A} - \hat{\mathbf{A}} = \begin{bmatrix} 0 & 0 & 0 & \frac{L_m}{\sigma \cdot L_S \cdot L_R} \\ 0 & 0 & -\frac{L_m}{\sigma \cdot L_S \cdot L_R} & 0 \\ 0 & 0 & 0 & -1 \\ 0 & 0 & 1 & 0 \end{bmatrix} \cdot \tilde{\omega}_R = \mathbf{A}_\omega \cdot \tilde{\omega}_R \tag{10}$$

The positive certain Lyapunov function is defined as Eq.11

$$V = \frac{1}{2}(S^2 + \frac{\tilde{\omega}_R^2}{a_\omega}) \tag{11}$$

With $\tilde{\omega}_R = \omega_R - \hat{\omega}_R$.
The time derivation of Lyapunov function in Eq.12

$$\dot{V} = S^T.S + \frac{1}{a_\omega}\tilde{\omega}_R\dot{\tilde{\omega}}_R \tag{12}$$

The time derivation of the Lyapunov function must be a negative definite function to meet the global asymptotic stability requirement. Therefore, we obtain the following results.

$$\begin{aligned} &\dot{\hat{\omega}}_R = \left(i_{S\alpha} - \hat{i}_{S\alpha}\right) \cdot \hat{\psi}_{R\beta} - \left(i_{S\beta} - \hat{i}_{S\beta}\right) \cdot \hat{\psi}_{R\alpha} \\ &\text{Or} \quad \hat{\omega}_R = \int z \cdot dt \end{aligned} \tag{13}$$

It also means that the speed estimator implemented according to the diagram in Fig. 1 only has the I-derivative controller, and it will not have the advantages of the P-proportional and the D-derivative controller shown in the diagram in Fig. 2. To improve the accuracy and stability, proportional and derivative components are added to have all the advantages of the PID controller so that we get a new speed estimator as follows:

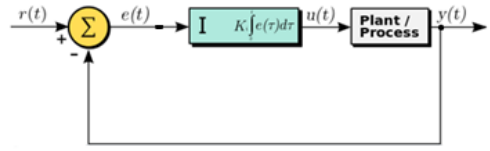

Fig. 1: The Integral (I) controller.

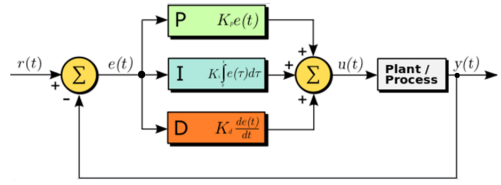

Fig. 2: The PID controller (I).

$$\hat{\omega}_R = K_{P\omega}.z + K_{I\omega}.\int z.dt + K_{D\omega}\frac{dz}{dt} \tag{14}$$

The components in the gain matrix are selected as in expression Eq.15.

$$
\begin{aligned}
g_1 &= 2 \cdot b \\
g_2 &= 0 \\
g_3 &= \left(2 \cdot L_m - \frac{L_S \cdot L_R}{L_m}\right) + \left(\frac{L_R}{L_m}\right) \cdot b \cdot R_R \cdot \\
&\quad \left((L_m)^2 - L_S \cdot L_R\right) + \frac{L_R \cdot \left(R_R \cdot R_S - w_b^2 \cdot L_m^2\right)}{R_R^2 + w_b^2 \cdot L_R^2} \\
g_4 &= \frac{b \cdot w_b \cdot L_R \cdot \left((R_R + b \cdot L_R) \cdot L_m^2\right)}{(R_R^2 + w_b^2 \cdot L_R^2) \cdot L_m} + \\
&\quad \frac{b \cdot w_b \cdot L_R \cdot \left((R_S - b \cdot L_S) \cdot L_R^2\right)}{(R_R^2 + w_b^2 \cdot L_R^2) \cdot L_m}
\end{aligned}
\tag{15}
$$

The desired performance of a sliding mode observer can be derived by selecting appropriate b values.

2.2. The SMO model of the induction motor

From the mathematical model of the induction motor and the speed sliding observer presented in Section 1, the suggested block diagram that incorporates the sliding mode observer and vector control is proposed Fig. 3. The current sensors are used to measure the two phase currents of the induction motor drives i_{sa} and i_{sb} in the suggested block. Then, at that point, they are changed into two parts of the stator current vector in the stator coordinate framework $i_{S\alpha}$, $i_{S\beta}$. The sliding mode observer (SMO) uses these current elements as inputs to calculate the rotor speed $\widehat{\omega}_m$. A current model uses them as inputs to estimate the elements of rotor flux $\psi_{R\alpha}$ and $\psi_{R\beta}$. Additionally, the current elements in the rotor coordinate system i_{Sx}, i_{Sy} and the current elements in the oriented coordinate system i_{Sd}, i_{Sq} are calculated using the current elements i_{Sa}, i_{Sb}. The SMO speed estimator replaces the actual speed determined by the encoder.

2.3. The Particle Swarm Optimization (PSO) Algorithm

The PSO algorithm is widely used in control systems [19] and [20]. In it, the trajectory of each individual in the search space is calibrated by changing the velocity of each individual, through its flight experience and the flight experience of other individuals in the search space. The position vector and velocity vector of an i^{th} individual in the multidimensional space are:

$$v_{ij} = wv_{ij} + c_1 r_1 (pbest_{ij} - x_{ij}) + c_2 r_2 (gbest - x_{ij}) \tag{16}$$

$$x_{ij} = v_{ij} + x_{ij} \tag{17}$$

$$w = w_{\max} - (\frac{iter}{maxiter})(w_{\max} - w_{\min}) \tag{18}$$

At each iteration, an element's velocity is determined by both the individual and the entire group experience.
Where v_{ij} is the velocity vector of the i^{th} individual; x_{ij} is the position of the i^{th} individual; pbest is the best position of each considered individual at present; gbest is the best position among the population; c_1 and c_2 are the acceleration constants; r_1 and r_2 are two random numbers with uniform distribution in the range [0, 1]; $w_{\max}$ is a final weigh; $w_{\min}$ is an initial weigh; Maxiter is the maximum iteration number; iter is the current iteration number.
Step of the PSO algorithm:
step 1: Define Objective Function, the PSO Parameters, initialization of position and velocity
step 2: Function Evaluation
step 3: Compute pbest and gbest
step 4: Update Velocity and Position handing boundary Constraints
step 5: Store Best Value
The flowchart of the PSO algorithm is shown in Fig. 4.

3. Results and discussion

The IM used for the simulation in MATLAB SIMULINK has elementary parameters: P =1.5 kW, U_{dc} =300V, P_P=2, R_S =1.28Ω, R_r =1.52Ω, L_m =0.129H, L_S =0.008H, L_r

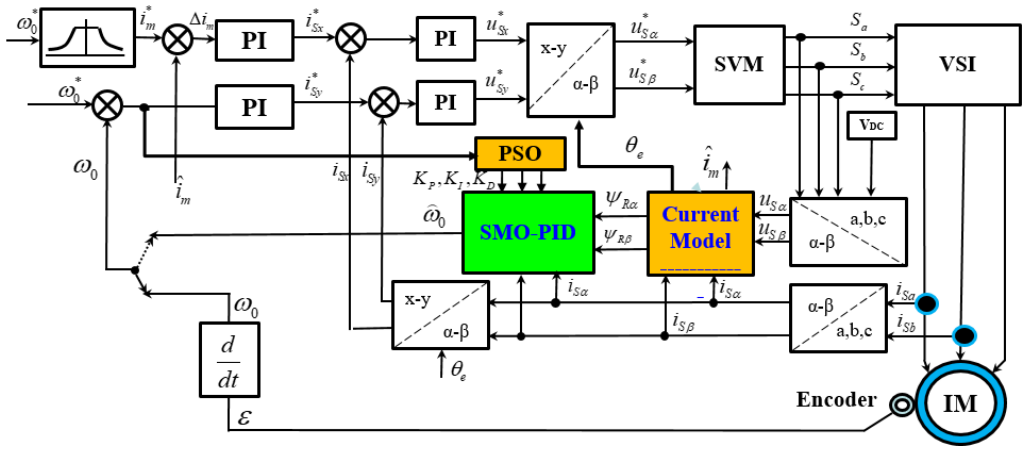

Fig. 3: The SMO-PID's control structure for an IM drive.

=0.008H, J=0.043 kg.m^2.

In this section, three distinct speed levels are simulated: 200 rpm, 100 rpm, and -100 rpm.

3.1. Speed Control of IM Drives:

In Fig. 5, the blue line is the desired speed, and the red line is the actual speed of the induction motor. The load torque acts at times from 0.2s to 0.3s and from 0.75 to 0.85. When the load appears, the speed response changes.

3.2. The sliding mode speed observer combined with conventional PID:

In the first place, the values K_p, K_i, K_d in the PID controller which is picked by trial and error are: K_p=5, K_i=10, K_d=0.005. The speed response that includes the reference speed, the actual rotor speed, and the SMO estimated speed in this case is shown in Fig. 6.

The error between the SMO estimated speed with the above parameters and the actual speed by the SME method in Fig. 7 is 6.5530 (m).

The above-estimated result is not good, so we try to find other better values of PID parameters, we finally choose K_p=100, K_i=10000, K_d=0.001. We perform the simulation again and get the estimated speed response by SMO method as shown in Fig. 8, and the error between estimated speed and actual speed is shown in Fig. 9. We see better results, the error is improved and the error value is 0.3496 (m).

3.3. The sliding mode speed observer combined with the PID with parameters optimized using the PSO algorithm:

It takes a lot of time and many times to find the values of K_p, K_i, K_d of the PID controller, the results are better but not the optimal parameters. In this section PSO algorithm is used to find the optimal parameters for PID controller. The main steps to find the optimal parameters for the PID controller are shown in Fig. 10.

The cost function in the PSO algorithm is the difference between the estimated speed value and the actual speed calculated by the MSE error as the expression below Eq.19.

$$S = \frac{1}{n}\sum_{1}^{n}(S_{real\_speed} - S_{SMO\_estimated\_speed})^2 \tag{19}$$

In the implementation of the PSO algorithm, the selected parameters are listed in Tab. 1. After implementing the PSO algorithm, we

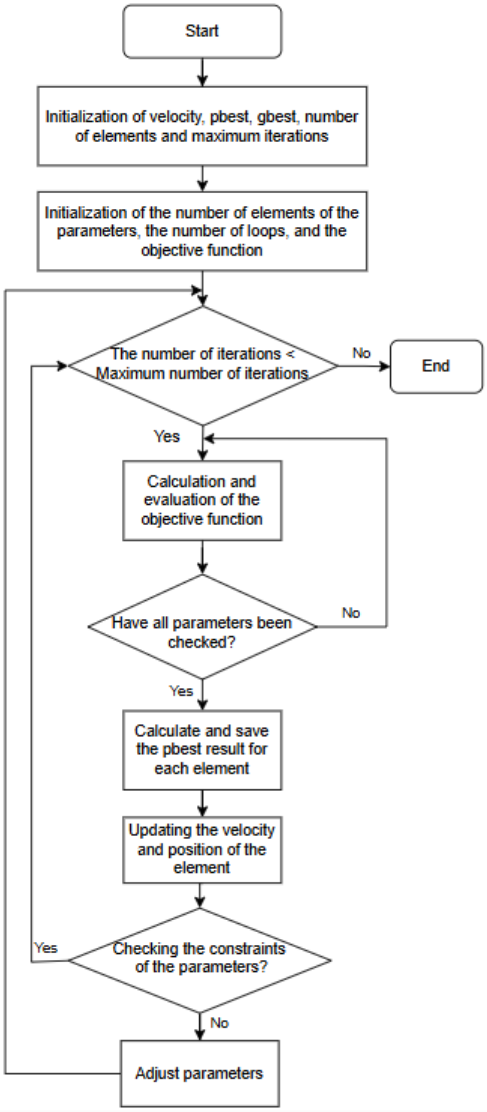

Fig. 4: The PSO algorithm steps.

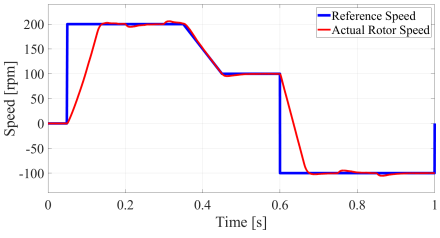

Fig. 5: Reference and actual rotor speed of the IM drive.

obtained the results in 20 iterations listed in Table 2.

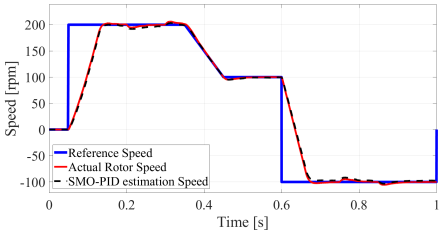

Fig. 6: The SMO estimated speed and actual rotor speed of the IM drive (in the first case).

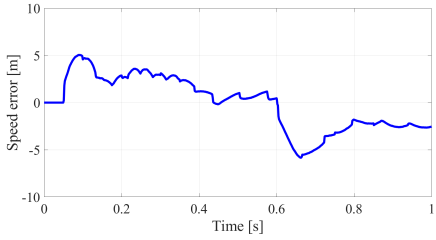

Fig. 7: Error between the SMO estimated speed and actual rotor speed of the IM drive (in the first case).

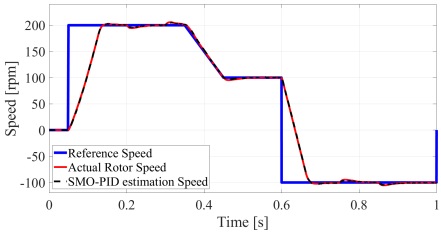

Fig. 8: The SMO estimated speed and actual rotor speed of the IM drive (in the second case).

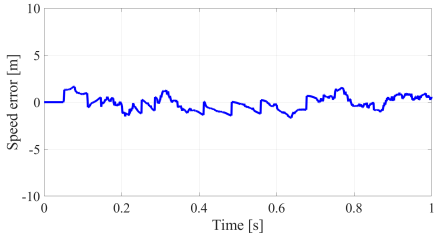

Fig. 9: Error between the SMO estimated speed and actual rotor speed of the IM drive (in the second case).

In addition to the results obtained in Table 2, the graph showing the relationship between 20 runs and the value of the cost function is drawn in Fig. 11.

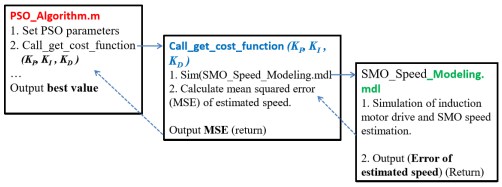

Fig. 10: The flowchart of the search for optimal parameters for the PID controller.

Tab. 1: The parameters of PSO algorithm.

Parameters	Values
Individual size	6
Number of iteration	20
c_1,c_2	1, 1
w_{max}, w_{min}	0.9, 0.4
Limit of K_p	1-500
Limit of K_i	100-30000
Limit of K_d	0.00001-0.0005

Tab. 2: The convergence results after 20 iterations.

Index	K_p	K_i	K_d	Objective function values
1	127.9594	23876.7006	0.0005	0.0137
2	128.3316	23876.8911	0.0005	0.0123
3	128.64	23877.0489	0.0005	0.011
4	128.64	23877.0489	0.0005	0.011
5	128.64	23877.0489	0.0005	0.011
6	128.64	23877.0489	0.0005	0.011
7	128.64	23877.0489	0.0005	0.011
8	128.64	23877.0489	0.0005	0.011
9	128.64	23877.0489	0.0005	0.011
10	128.64	23877.0489	0.0005	0.011
11	127.0933	24175.8731	0.0005	0.0094
12	127.0933	24175.8731	0.0005	0.0094
13	127.0933	24175.8731	0.0005	0.0094
14	127.0933	24175.8731	0.0005	0.0094
15	127.0933	24175.8731	0.0005	0.0094
16	127.0933	24175.8731	0.0005	0.0094
17	127.0178	24169.2362	0.0005	0.0094
18	127.0178	24169.2362	0.0005	0.0094
19	122.9789	24219.3984	0.0005	0.009
20	121.2348	24241.1126	0.0005	0.0086

From the data table as well as the graph, it shows that in the first rounds, the values of the parameter sets K_p, K_i, K_d are not very good, but the following rounds are better because the value of the cost function is small and the 20th time is the best value after 20 loops.

The parameters found in the final run are K_p= 121.234847092909, K_i= 24241.1125696315, K_d = 0.0005.

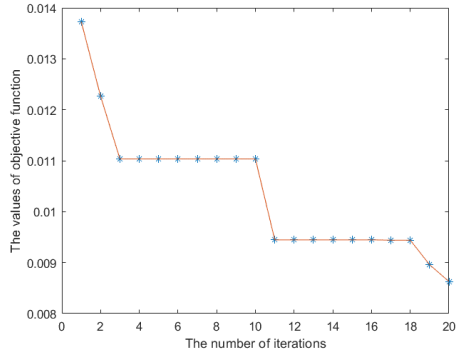

Fig. 11: Convergence graph of the PSO algorithm after 20 iterations.

And this is also the most optimal value in 20 iterations. We use these parameters to perform the simulation again. The results are shown in Fig. 12 and Fig. 13. The results shown in Fig.

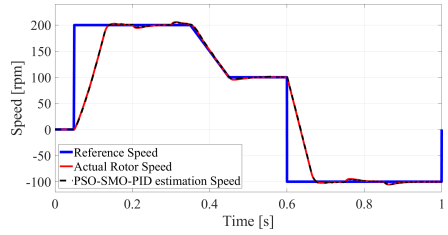

Fig. 12: The SMO estimated speed and actual rotor speed of the IM drive (in the case using PSO algorithm).

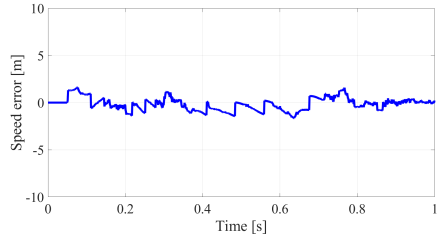

Fig. 13: Error between the SMO estimated speed and actual rotor speed of the IM drive (in the case using PSO algorithm).

12 and Fig. 13 show that the PSO-SMO speed estimator is much better than the traditional SMO estimator and the error in this case is also

significantly smaller. Its error, in this case, is 0.0086 (m).

3.4. Result comparison between the two methods SMO-PID speedy estimate and PSO-SMO-PID speedy estimate

After simulating the traditional methods and the proposed method, the results are summarized in Table 3. In Table 3, the first column

Tab. 3: Comparison of effectiveness of the proposed method with traditional method.

Method	K_p, K_i, K_d	Speed error
SMO-PID. [17]	5.0000, 10.0000, 0.0050	6.553
SMO-PID. [18]	100.0000, 10000.0000, 0.0010	0.3496
PSO-SMO-PID	121.2348, 24241.1126, 0.0005	0.0086

lists the research methods, the second column is the corresponding parameters K_p, K_i, K_d, and the third column is the value of the cost function calculated by the sum of average squares (SME) method. In the first time, the result is not good, the next time the result is better but not the optimal value. With the PSO-SMO-PID speed estimation method, the results are many times better than the traditional method.

4. Conclusion

This paper presents a method of estimating the speed of the IM motor using the SMO method combined with the PID controller. In which the parameters of the PID controller are selected according to the traditional method (trial and error) and searched by the PSO algorithm.

The simulation results show that the SMO-PID traditional speed estimation method is time-consuming and inefficient, the PSO-SMO-PID speed estimation method is very effective with significantly small errors, saving time (due to the powerful processor and the intelligent algorithm PSO). This demonstrates the superiority of the proposed method in finding the optimal parameters of the PSO-SMO-PID speed estimation method compared to the traditional SMO-PID method.

5. Acknowledgement

Sponsorship or financial support acknowledgment should be included here.

References

[1] T. Orlowska-Kowalska and M. Dybkowski. Stator-current-based mras estimator for a wide range speed-sensorless induction-motor drive. *IEEE Trans. on industrial electronics*, 57(4):1296–1308, 2009.

[2] L. Sbita and M.B. Hamed. An mras–based full order luenberger observer for sensorless drfoc of induction motors. *Int. J. ACSE*, 7(1):11–20, 2007.

[3] S. Mondal and C. Mahanta. A fast converging robust controller using adaptive second order sliding mode. *ISA transactions*, 51(6):713–721, 2012.

[4] R. Mini, B.P. Shabana, B.H. Satheesh, and M.N. Dinesh. Low speed estimation of sensorless dtc induction motor drive using mras with neuro fuzzy adaptive controller. *Int. J. Electr. Comput. Eng. (IJECE)*, 8(5):2691–2702, 2018.

[5] T.C. Tran, P. Brandstetter, and H.H. Vo. The sensorless speed controller of induction motor in dfoc model based on the voltage and current. *J. Adv. Eng. Comput.*, 3(1):320–328, 2019.

[6] J. Chen, J.Huang, and Y.Sun. Resistances and speed estimation in sensorless induction motor drives using a model with known regressors. *IEEE Trans. on Ind. Electron.*, 66(4):2659–2667, 2018.

[7] T.C. Tran, P. Brandstetter, H.H. Vo, C.S.T. Dong, and M. Kuchar. Comparison of the speedy estimate methods of the induction motors. *ELKOMNIKA (Telecommun. Comput. Electron. Control.)*, 21(1):223–234, 2022.

[8] J. Kim, Y. Lee, and J. Lee. A sensorless speed estimation for indirect vector control of three-phase induction motor using extended kalman filter. *In 2016 IEEE Reg. 10 Conf. (TENCON)*, pages 3087–3090, 2016.

[9] M.L. Jayaramu, H.N. Suresh, M.S. Bhaskar, D. Almakhles, S. Padmanaban, and U. Subramaniam. Real-time implementation of extended kalman filter observer with improved speed estimation for sensorless control. *IEEE Access*, 9:50452–50465, 2021.

[10] V.I. Utkin. Sliding mode control design principles and applications to electric drives. *IEEE Trans. Ind. Electron*, 31(4):737–743, 1995.

[11] G. Tarchala and T. Orlawska-Kowalska. Sliding mode speed observer for the induction motor drive with different sign function approximation forms and gain adaptation. *Organ Stowarzyszenia Elektrykow Polskish*, 1:13, 2020.

[12] D. Luenberger. An introduction to observers. *IEEE Trans. on automatic control*, 16(6):596–602, 1971.

[13] L. Zhao, J. Huang, H. Liu, B. Li, and W. Kong. Second-order sliding-mode observer with online parameter identification for sensorless induction motor drives. *IEEE Trans. on Ind. Electron.*, 61(10):5280–5289, 2014.

[14] C. Dong, P. Brandstetter, H.H. Vo, and V.H. Duy. Sliding mode observer for induction motor control. *AETA 2015: Recent Adv. Electr. Eng. Relat. Sci. Springer Int. Publ.*, pages 313–323, 2016.

[15] F. Mehazzem, A. Reama, and H. Benalla. Online rotor resistance estimation based on mras-sliding mode observer for induction motors. *In 4th Int. Conf. on Power Eng. Energy Electr. Drives. IEEE*, pages 828–833, 2013.

[16] T.C. Tran, P.Brandstetter, C.D. Tran, S.D. Ho, M.C.H. Nguyen, and P.N. Phuong. Parameters estimation for sensorless control of induction motor drive using modify ga and csa algorithm. *AETA 2018 Recent Adv. Electr. Eng. Relat. Sci. Theory Appl. Springer Int. Publ.*, pages 580–591, 2020.

[17] P. Vas. Vector control of ac machines. *Retrieved from Clarendon press, Oxf.*, 1990.

[18] T.C. Tran, P. Brandstetter, and M. Kuchar. Application of optimal solutions in field-oriented control of induction motor. in induction motors-recent advances. *New Perspect. Appl. IntechOpen. Retrieved from https://www.intechopen.com/chapters/1134665*, 2023.

[19] T. Banerjee, S. Choudhuri, J.Bera, and A. Maity. Off-line optimization of pi and pid controller for a vector controlled induction motor drive using pso. *In Int. Conf. on Electr. & Comput. Eng. (ICECE 2010)*, pages 74–77, 2010.

[20] M. Rekha and K.K. Malligunta. Variable frequency drive optimization using torque ripple control and self-tuning pi controller with pso. *Int. J. Electr. Comput. Eng.*, 9(2):802, 2017.

About Authors

Thinh Cong TRAN was born in Da Nang City, Vietnam. He received his M.Sc. degree in Electrical and Electronic Engineering from National University of Technology, Ho Chi Minh City, Vietnam in 1998. He received his PhD degree in Electrical Engineering and Computer Science from VSB - Technical University of Ostrava, Czech Republic in 2018. Now, he is teaching at department of electrical and electronics engineering (FEEE), Ton Duc Thang University, Ho Chi Minh city, Vietnam. His research interests include microcontroller systems, power electronic, modern control methods of electrical drives, soft computing algorithms, and optics.

Hau Huu VO finished his Ph.D. at Ostrava Technical University (VSB-TUO), the Czech Republic in 2017. He is a Lecturer at the Faculty of Electrical and Electronic Engineering (FEEE), Ton Duc Thang University (TDTU), Vietnam. He published 05 journal articles and 10 conference papers. He is interested in intelligent electric motors, control, and robotics.

P. BRANDSTETTER was born in Ostrava, Czech Republic, 1955, 1 June. He received the M.Sc. and Ph.D. degrees in Electrical Engineering from Brno University of Technology, Czech Republic, in 1979 and 1987, respectively. He is currently a full professor in Electrical Machines, Apparatus and Drives and dean of Faculty of Electrical Engineering and Computer Science at VSB Technical University of Ostrava. Research activities include modern control methods of AC drives, for example, sensorless control of the IM and PMSM drives using different types of the observers.